RSC Advances

PAPER

View Article Online
View Journal | View Issue

Cite this: *RSC Adv.*, 2014, **4**, 1283

Local structure and piezoelectric instability in lead-free $(1-x)BaTiO_3$-$xA(Cu_{1/3}Nb_{2/3})O_3$ (A = Sr, Ca, Ba) solid solutions†

Deepam Maurya,*[a] Ashok Kumar,[b] Valeri Petkov,[c] James E. Mahaney,[d] Ram S. Katiyar[e] and Shashank Priya*[a]

Received 4th September 2013
Accepted 21st October 2013

DOI: 10.1039/c3ra44886j

www.rsc.org/advances

This study provides a fundamental understanding of the enhanced piezoelectric instability in ABO_3 perovskite based lead-free piezoelectric materials. For this we synthesized $(1-x)BaTiO_3$-$xA(Cu_{1/3}Nb_{2/3})O_3$ (A: Sr, Ba and Ca and $x = 0.0$–0.03) solid solutions exhibiting high piezoelectric response. The piezoelectric instability in these compositions was found to increase with x despite monotonous decrease in the long range polar ordering. High energy X-ray diffraction coupled with atomic pair distribution functions (PDF)s indicated an increase in local polarization. Raman scattering and EPR analysis revealed that substitutions on A and B sites both substantially perturbed the local octahedral dynamics and resulted in localized nano polar regions which imparted the high piezoelectric response.

Introduction

Piezoelectric materials with a broad range of functional properties are utilized in numerous applications such as high voltage sources, sensors, actuators, energy harvesters and nonvolatile memory elements.[1] However, most of these devices employ PZT based piezoelectric materials. Environmental restrictions require elimination of lead from all the consumer electronics. In spite of continuous research efforts, there has been limited success in achieving high piezoelectric response in known lead-free piezoelectric systems. Recently, $K_{0.5}Na_{0.5}NbO_3$ (KNN) and $Bi_{0.5}Na_{0.5}TiO_3$ (NBT) based lead-free piezoelectric ceramics have attracted much attention. However, KNN based piezoelectric materials utilize expensive Nb_2O_5 for synthesis, which increases cost of the process. Also, KNN based materials are sensitive to moisture and have sintering issues due to volatile nature of alkali elements. On the other hand, $Bi_{0.5}Na_{0.5}TiO_3$ (NBT) is characterized by smaller value of piezoelectric response $d_{33} \sim 80$ pC N^{-1}. Most of the lead-free piezoelectric candidates are based on ABO_3 type perovskite structure and compositional modification of ABO_3 type piezoelectric materials has been a principal technique used for tuning the magnitude of electromechanical response.[2] These compositional modifications perturb the atomic-scale structure and global microstructure, and sometimes modulate the phase transition behavior showing relaxor-type diffuse phase transition (DPT).[3,4] Thus, it is imperative to understand the role of A and B-site substitutions on functional response for designing lead-free piezoelectric materials with enhanced characteristics.

Despite various theoretical and experimental investigations,[5,6] it is still debatable how small doping perturbations on A- and B-site changes the local structure and consequently macroscopic properties. To understand the role of A-site and B-site substitutions, archetype $BaTiO_3$ were selected, which is one of the widely studied piezoelectric/ferroelectric materials. $BaTiO_3$ was blended with dilute concentrations of $Ba(Cu_{1/3}Nb_{2/3})O_3$(BCN), $Sr(Cu_{1/3}Nb_{2/3})O_3$(SCN), and $Ca(Cu_{1/3}Nb_{2/3})O_3$ (CCN). The perovskite type $Ba(Cu_{1/3}Nb_{2/3})O_3$ (BCN) material possesses tetragonal unit cell with lattice parameters $a = 4.0464$ Å and $c = 4.1807$ Å ($c/a = 1.033$) [ref. 7]. Blending of these complex perovskite materials with $BaTiO_3$, resulted in lead-free piezoelectric compositions with high piezoelectric response ($d_{33} \sim 330$ pC N^{-1} and $k_p \sim 46\%$). This value of piezoelectric response was comparable to that of commercial (Ferroperm) PZT (Pz23) with $d_{33} = 330$ pC N^{-1} and $k_p = 0.52$. The Goldschmidt's tolerance factor of these compositions was found to change linearly and so was the tetragonality. Interestingly, the change in piezoelectric response was nonlinear resulting in maximum at certain intermediate compositions. B-site off centering displacement controls the tetragonality and is only weakly dependent on the A-site displacements.[5] This implies the contribution of local

[a]*Center for Energy Harvesting Materials and Systems (CEHMS), Bio-Inspired Materials and Devices Laboratory (BMDL), Virginia Tech, Blacksburg, VA 24061, USA. E-mail: mauryad@vt.edu; spriya@vt.edu*

[b]*National Physical Laboratory, Council of Scientific and Industrial Research (CSIR), New Delhi 110 012, India*

[c]*Department of Physics, Central Michigan University, Mount Pleasant, Mich, 48859, USA*

[d]*Edward Via College of Osteopathic Medicine, Blacksburg, VA 24060, USA*

[e]*Department of Physics and Institute for Functional Nanomaterials, University of Puerto Rico, San Juan, Puerto Rico 00931-3343*

† Electronic supplementary information (ESI) available. See DOI: 10.1039/c3ra44886j

structural distortions due to B-site substitutions towards enhanced piezoelectric response.

In the present work, we investigated the role of A and B-site substitution towards local structural changes and its correlation with the enhanced piezoelectric response. Atomic pair distribution function (PDF) and Raman spectroscopy are the powerful tools for the study of local structure in crystalline, quasicrystalline and non-crystalline materials, providing information about the atomic and nano-scale structures of materials. Raman spectroscopy provides vital information about the changes in lattice vibrations, which are collective entities that directly govern the macroscopic ferroelectricity [ref. 8]. The local changes in A–O bonds alter the macroscopic ferroelectricity by modifying the fluctuation in octahedral rotation modes. However, Raman spectrum does not provide much information about the local environment of copper ions in present system. To further probe the local environment of Cu dopant, electron paramagnetic resonance (EPR) spectra were recorded at room temperature (RT), which clearly indicated the perturbation of B-site environment with A-site substitution. The results provide understanding about the origin of enhanced piezoelectric instability and the local structural changes in ABO_3 type complex lead-free perovskite solid solutions given by the formulation $(1-x)BaTiO_3$-$xA(Cu_{1/3}Nb_{2/3})O_3$ (BT-xACN, $x = 0.0$–0.03, A = Ba, Sr, Ca). The temperature dependence of the relative permittivity was used to calculate the diffuseness parameter (critical exponent) for understanding the modulation in ferroelectric phase transition behavior due to the substitutions on A-site and B-site. We believe that the present work will provide a new understanding of lead-free piezoelectric materials that will be helpful in designing better compositions.

Experimental

Synthesis of $(1-x)BaTiO_3$-$xA(Cu_{1/3}Nb_{2/3})O_3$ (x = , 0.0, 0.01, 0.015, 0.02, 0.025, 0.03 and 0.035) with A: Ba, Sr, Ca ceramics were performed using conventional solid state method.[9] We do not expect change in stoichiometry of the materials or significant weight loss after sintering process due to absence of volatile elements. All the sintered pellets were found to have more than 95% of theoretical density. Traditional powder XRD patterns were recorded to confirm the phase evolution in all samples using PANalytical X'Pert Pro powder X-ray diffractometer with CuKα radiation ($\lambda = 1.5418$ Å). All the specimens were found to crystallize in pure perovskite phase. The high energy powder X-ray diffraction patterns were recorded at RT using Ag-Kα ($\lambda = 0.559$ Å) radiation for pure $BaTiO_3$ and some selected specimens from the three series of compositions. For electrical measurements, silver electrodes were applied on flat faces of sintered pellets. Computer controlled HP 4192A impedance analyzer coupled with high temperature oven was used to measure the dielectric response as a function of temperature at various frequencies with oscillation level of 500 mV. The ceramic disks were poled under DC electric field of 3–4 kV mm^{-1} in silicone oil bath for 1 h at RT. The longitudinal piezoelectric constant (d_{33}) values were measured using Berlincourt d_{33} meter (APC International) and planar electromechanical coupling constants (k_p) were measured by resonance anti-resonance method using HP 4194A impedance analyzer. Room temperature micro Raman studies were conducted in the backscattering geometry using a Jobin-Yvon T6400 Triplemate instrument utilizing laser radiation of 514.5 nm from a coherent Innova 99 Argon source. The green laser light was focused in ~2 μm diameter by using a Raman microprobe with a 50× objective. Electron paramagnetic resonance (EPR) spectra (X-band) were recorded using a Bruker ER 200D spectrometer, equipped with a TE_{102} cavity at room temperature (~21 °C).

Results and discussion

Fig. 1(a), (c) and (e) show the traditional XRD-patterns recorded at RT for various compositions of BT-xBCN, BT-xSCN and BT-xCCN, respectively. This data clearly demonstrates that all compositions crystallize in pure perovskite phase. The splitting of (200) Bragg reflections suggested tetragonal macroscopic symmetry indicative of the presence of long range ferroelectric ordering. The magnified view of the variation in (002) and (200)

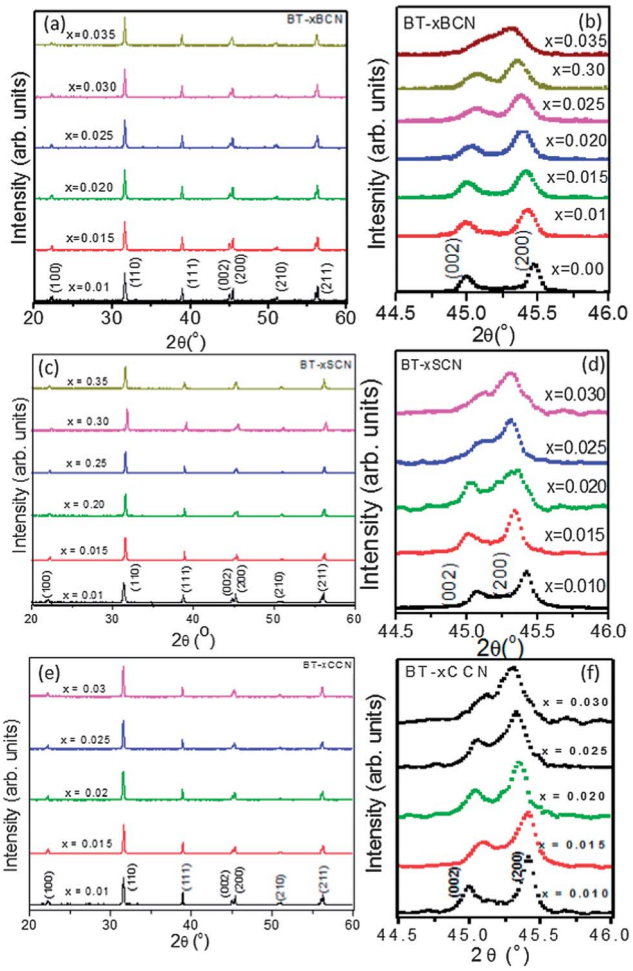

Fig. 1 XRD-spectra recorded at RT for BT-xACN with A-site ion as (a) Ba (c) Sr (e) Ca, variation in {200} Bragg reflections with A-site ion as: (b) Ba, (d) Sr, (f) Ca.

Bragg peaks with the change in compositions for all three series of samples is shown in Fig. 1(b), (d) and (f). As can be seen here with increasing value of x, the (002) Bragg peak shifts to higher values of 2θ and the (200) Bragg peak shifts towards the lower values of 2θ indicating increase in the value of the lattice parameter 'a' and decrease in the value of the lattice parameter 'c'. This suggests a monotonous decrease in the long range ferroelectric ordering in the corresponding systems. The d-spacing of (200) and (002) peaks was used to calculate the tetragonality (c/a) of the specimens. Fig. 2(a)–(c) show the variation of tetragonality (c/a) and grain size for all modified $BaTiO_3$ compositions. The grain size for pure $BaTiO_3$ was measured to be 28 μm (tetragonality (c/a) = 1.0104) which further increases up to 90 and 80 μm for $x = 0.01$ in BT-xBCN and BT-xSCN. The large grain size of Sr-doped $BaTiO_3$ is comparable to the values reported earlier.[10] Also, the small concentration of Nb and Cu substitution gives rise to large grain sizes.[11,12] On further increasing the values of x, the grain size decreases monotonously, which can be attributed to the increased concentration of Nb^{5+} and Cu^{2+} [ref. 13]. The average grain size for BT-xCCN compounds was found to be smaller than that of the compositions of the other two series.

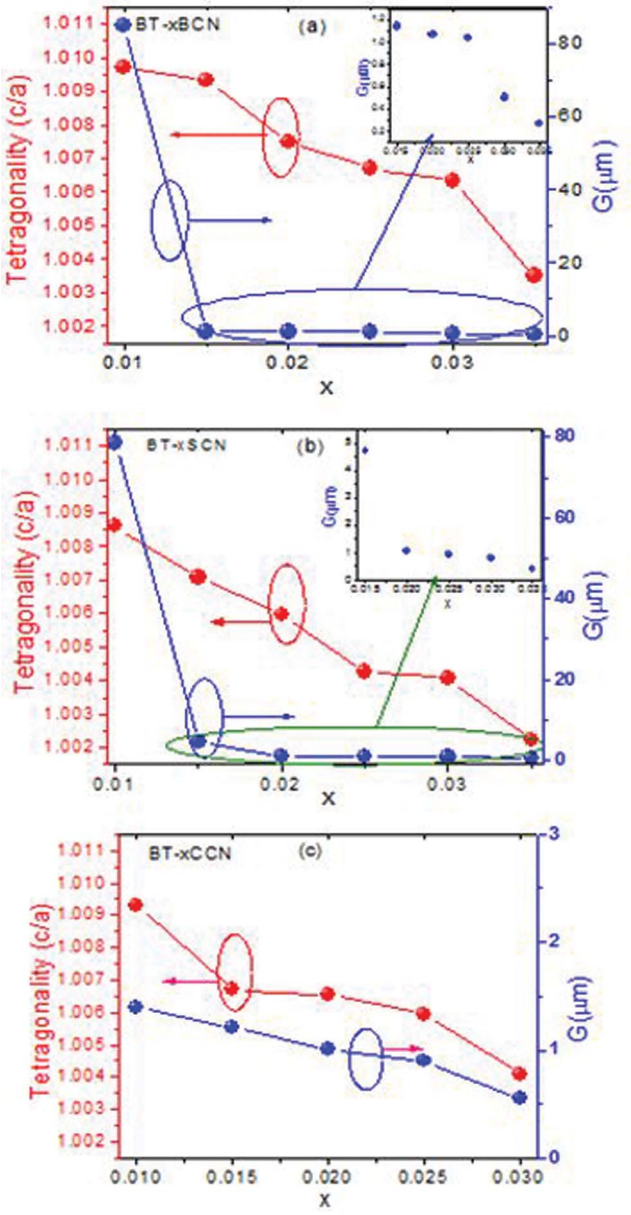

Fig. 2 Tetragonality and grain size as a function of composition in BT-xACN with A: (a) Ba (b) Sr and (c) Ca.

In order to understand the nature of the ferroelectric phase transition, we recorded the temperature dependence of the relative permittivity. Fig. 3 shows the temperature dependence of the relative permittivity and the loss tangent at 1 kHz for various compositions. It can be observed that with the increase in the values of x for all specimens, the *Curie* temperature (T_c) decreases and the *Curie* peak gets smeared reflecting an increasing diffuse nature of the phase transitions (DPT). However, the rate of shift of the Curie temperature towards RT is higher in case of BT-xCCN in comparison to BT-xBCN and BT-xSCN series. Moreover, the Curie peaks in case of BT-xBCN specimens are comparatively sharper than those of the compounds having same value of x in BT-xSCN and BT-xCCN series. The substitutions of Sr^{2+} and Ca^{2+} on the Ba-sites do not appear to favor long range ordering. The diffuse nature of the phase transition can be attributed to a perturbed localized dynamics and polar structural distortions of the octahedra due to the substitution on the A- and B-sites. The values of T_c and diffuseness parameter for various compounds are shown in Fig. 4.

Furthermore, the electromechanical response as a function of composition for whole series of samples is shown in Fig. 4(a) and (b). The magnitude of the longitudinal piezoelectric constant (d_{33}) and planar electromechanical coupling constants increases with x going through a maximum. The maximum d_{33} (330–333 pC N^{-1}) was found to occur at $x = 0.025$ for BT-xBCN and at $x = 0.015$ for BT-xSCN. In the case of BT-xCCN, the maximum $d_{33} \sim 260$ pC N^{-1} was found to occur at $x = 0.020$. The variation of the planar electromechanical coupling constant (k_p) with composition was similar to that of d_{33}. The highest electromechanical coupling constants of 43% and 46% were measured in $x = 0.025$ for BT-xBCN and $x = 0.015$ for BT-xSCN respectively. However, the BT-xCCN series was found to exhibit a relatively small value of $k_p \sim 35\%$. With the increase in the composition x, Curie temperature (T_c) was shifted towards room temperature (Fig. 4(c)) and the transition became rather diffuse as can be seen from the diffuseness parameter (Fig. 4(d)), which was calculated using modified Curie–Weiss law [ref. 1]. Increase in diffuseness parameter indicates the emergence of relaxor behavior in the system. We next performed high energy X-ray diffraction analysis coupled with atomic PDFs analysis on selected specimens to understand the local structure.

Recently high-energy XRD and atomic PDF analysis has gained tremendous importance towards the understanding of the local structure of functional materials and its correlation with their functional properties.[14] The PDF is defined as[14]: $G(r) = 4\pi r[\rho(r) - \rho_o]$, where $\rho(r)$ and ρ_o are the local and average atomic number densities, respectively, and r is the radial distance. The value of atomic PDFs comes from the fact that

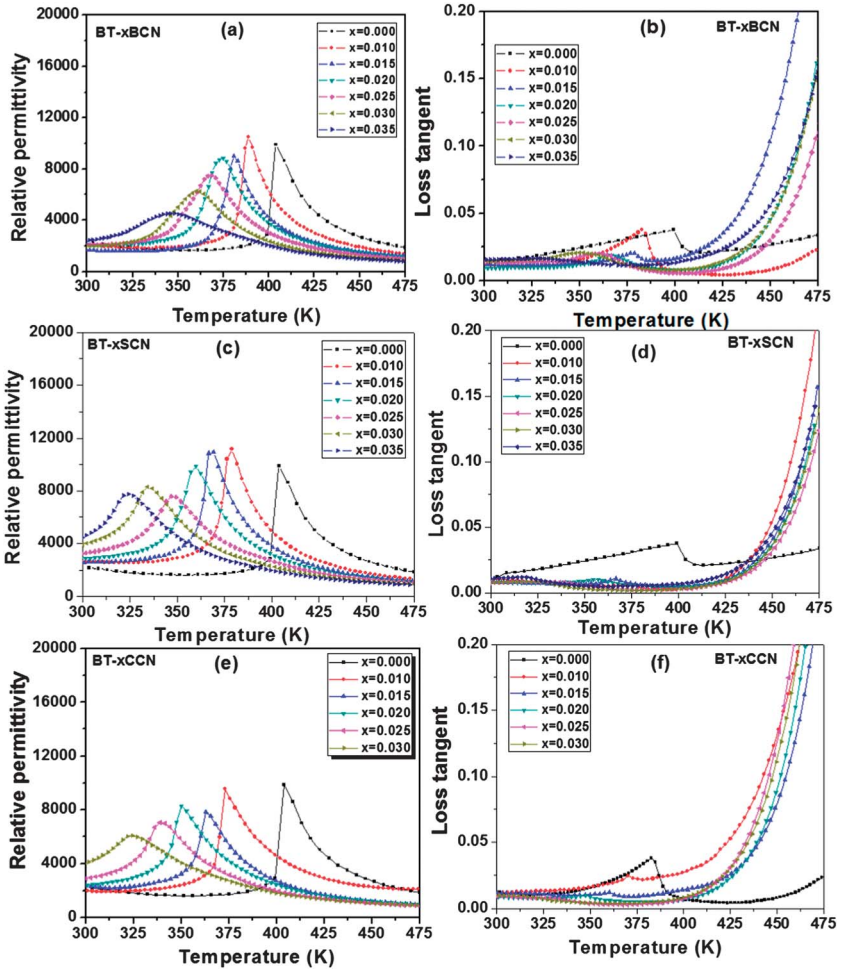

Fig. 3 Temperature dependence of dielectric response at 1 kHz for various compositions of BT-*x*ACN with A as (a and b) Ba, (c and d) Sr,(e and f) Ca.

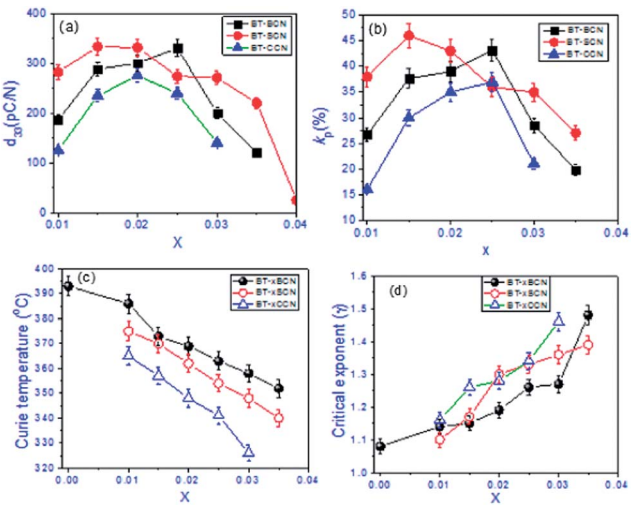

Fig. 4 Compositional dependence of (a) d_{33}, (b) k_p (%), (c) Curie temperature (T_c), (d) critical exponent (γ) for BT-*x*ACN (with A = Ba, Sr and Ca).

they consider all components of the diffraction patterns, including sharp Bragg peaks and diffuse scattering, and so are sensitive both to the average and local atomic-scale structure. Also, atomic PDFs do not imply any periodicity so that materials of any degree of structural coherence are possible to be studied on the same footing. The experimental PDFs peak at real space distances, where well defined atomic pairs exist and can be easily used to test and refine structural models.

The PDF for pure $BaTiO_3$ and its derivatives were found to show a series of well-defined peaks to high interatomic distances reflecting the presence of a sequence of well-defined coordination spheres in these crystalline materials (Fig. 5). The PDF for pure $BaTiO_3$ was matched very well with a structural model featuring a tetragonal perovskite structure with space group *P4mm* (Fig. 5). The high-*r* part of the experimental PDFs is depicted in Fig. 6. Due to the cooperative off-centering of Ti atoms in the tetragonal/polar phase the intensity distribution of several peaks in the atomic PDFs (red line) is different from that in the PDF (blue line) for the cubic/non-polar phase. For example, in the cubic phase, the PDF doublet at 26 Å has its low-*r* component stronger in intensity than the higher-*r* component. Again in the cubic phase, the PDF doublet at 28 Å has its

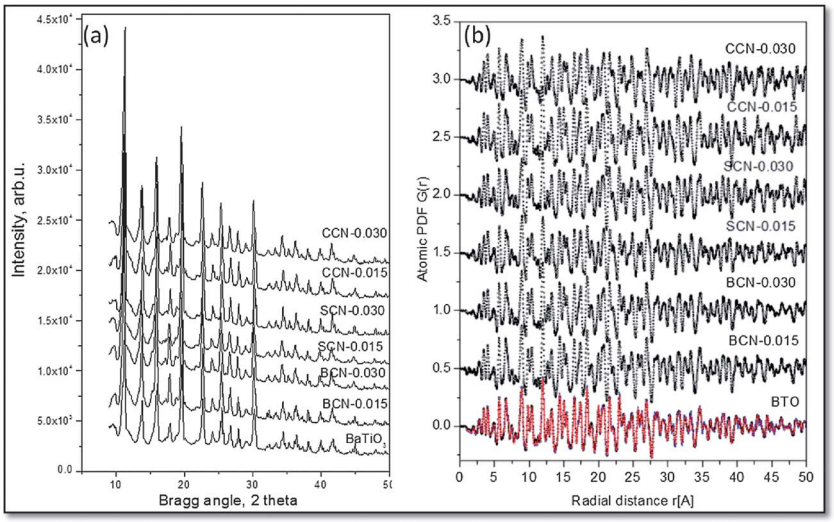

Fig. 5 (a) Experimental XRD patterns taken with Ag Ka ($\lambda = 0.559$ Å) radiation. Note XRD data quality is optimized for atomic PDFs analysis, (b) experimental atomic PDFs. The PDF for $BaTiO_3$ (BTO) is very well reproduced by a model (line in red) based on a tetragonal (polar/ferroelectric) structure.

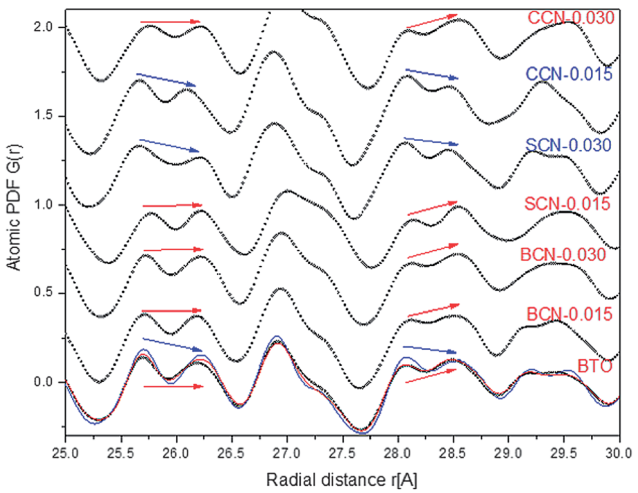

Fig. 6 Higher-*r* part of the experimental atomic PDFs (symbols). Model PDFs for tetragonal (line in red) and cubic (line in blue) structures of BTO are shown as well. Note the different behavior of particular PDF peaks in the case of polar (tetragonal) and non-polar (cubic) structures. The PDF peaks at 25.7 A and 26.25 A for the polar structure have similar intensity (follow the red arrow) while those in the PDF of the non-polar structure go like high-low intensity (follow the blue arrow).

low-*r* component stronger in intensity when compared to the higher-*r* one. The situation is very different with the polar/tetragonal phase. Here the PDF doublet at 26 Å has two components of equal intensity, and the intensity distribution in the PDF doublet at 28 Å is reverse when compared to the case of the non-polar phase. These observations are summarized using blue descending arrows for the case of a non-polar/cubic phase and red ascending arrows for the case of a polar/tetragonal phase and used here to differentiate between them. Note a similar analysis based on PDF data for $BaTiO_3$ has been reported by Petkov *et al.*[15]

The PDF peaks at 25.7 and 26.25 Å for the polar structures have similar intensity while those in the PDF of the non-polar structure go like high-low (follow the blue arrows). Moreover, the PDF peaks at 28.25 Å and 28.5 Å for the polar structure go like low-high intensity (follow the arrows in red) while those in the PDF for non-polar go like high-low. From this PDF data it can be seen that the polar distortions survive and even become somewhat stronger with increasing composition in BT-*x*BCN, survive in SCN_15 (BT-0.015SCN) but not in SCN_30 (BT-0.030SCN) and in CCN_15 (BT-0.015CCN) but reemerge in CCN_30 (BT-0.030CCN). Thus at lower concentrations of Cu^{2+} and Nb^{5+}, the substitution of Sr^{2+} on Ba^{2+}-site maintains increased polar character of the specimen (SCN_15). However, the substitution of Ca^{2+} having smaller ionic radii reduces the polar nature of the corresponding specimen (*i.e.* CCN_15) due to the constrained off-centering of B-site cations. On the other hand, for the specimens (*i.e.* CCN_30) with higher concentration of Cu and Nb, the substitution of Ca on Ba-site maintains the polar character due to their synergic effect. Being smaller in size, at higher concentration, substitution of Ca on B-site cannot be ruled out [ref. 16]. This substitution would lead to the increased distortion at local length scales. This result is in line with the pronounced hyperfine splitting observed in higher magnetic field regime of EPR spectrum of heavily Ca substituted specimen CCN_30 as discussed in a forthcoming paragraph. Furthermore, the 4d transition ions (Nb^{5+}) are more covalently bounded to oxygen than 3d transition ions resulting in a strong off-centered axially perturbed octahedral crystal field[17] influencing the local phonon dynamics as explained by Raman scattering results. The increased polar nature explains the enhanced piezoelectric instability in BT-*x*BCN and BT-*x*SCN compositions. At a certain small grain size, domain motion is confined by the geometrical restrictions and the system subsequently loses piezoelectric response. We anticipate that the same phenomena occurs in BT-*x*CCN where despite high local

polar character revealed by the experimental PDF data, a decrease in the piezoelectric response is observed for $x = 0.03$ composition. To further understand the perturbation of the localized dynamics, polar distortions and their correlation with the piezoelectric instability, Raman spectroscopy was employed.

Raman spectroscopy is a versatile technique for detection of subtle structural distortions in perovskites and an excellent probe for the local structure due to its shorter characterization length. At RT tetragonal $BaTiO_3$ has C_{4v} symmetry, which allows $3(A_1 + E) + 1(B_1 + E)$ Raman active optical modes and $1(A_1 + E)$ acoustic modes. There is further splitting in A_1 and E modes to transverse optic (TO) and longitudinal optic (LO) modes due to the long-range electrostatic force associated with lattice ionicity. In tetragonal $BaTiO_3$ phase, Raman active modes are: $3A_1(TO) + 3A_1(LO) + 3E(TO) + 3E(LO) + 1E(LO + TO) + 1B_1$. Further optical modes can be seen in the Raman spectra due to dielectric anisotropy (Fig. 7).

Fig. 7(a)–(c) shows the Raman spectra for various compositions of BT-*x*ACN (Ba, Sr and Ca). Raman spectra of pure $BaTiO_3$ ($x = 0$) depicts an over-damped transverse mode $E_1(TO)$ as observed by continuous increase in the scattered intensity below 150 cm^{-1}. The $A_1(TO_1)$, $A_1(TO_2)$, $A_1(TO_3)$ and $A_1(LO_3)$ modes were observed at ~170, 272, 517 and 720 cm^{-1}, respectively. The interference of the sharp $A_1(TO_1)$ mode at 170 cm^{-1} with the broad $A_1(TO_2)$ mode at 272 cm^{-1} results in an anti-resonance effect in terms of a dip at ~181 cm^{-1}. The $E(TO_2)$ mode was observed at 305 cm^{-1}. In solid solution of BT-*x*ACN, Sr^{2+} and Ca^{2+} easily occupy A-site (Ba^{2+}-site) whereas B-site (Ti^{4+} (0.605 Å)) octahedra becomes more complex with the substitution of Cu^{2+} and Nb^{5+} which in turn gives splitting in the phonon modes between 700 and 800 cm^{-1} (see Fig. 7(a)–(d)). Interestingly, a mode with very small intensity appears in the high frequency regime ~840 cm^{-1} for the A-site substituted specimens (BT-*x*SCN and BT-*x*CCN). The modes at 170, 305 and 720 cm^{-1} are signature of the long-range ferroelectric ordering. It can be seen that with the increase in *x* values, these modes subside. This change is consistent with the decrease in the tetragonality as observed in the XRD spectra which was accompanied with reduction in the grain size for heavily doped compositions and shifting of T_c towards RT. Furthermore, the confinement of phonons in materials with distorted octahedra and small grains leads to a breakdown of the long range order, allowing phonons not belonging to the center of the Brillouin zone ($k \sim 0$) to become active leading to broadening of the Raman modes.[18,19] Also, the lower frequency Raman mode was found to soften with the increase in compositions '*x*' (Fig. 8). The rate softening of the mode was higher for the specimen with Ba and Sr on A-site for lower concentrations. The softening of mode signifies that the system is being driven towards phase transition. However, the substitution of Ca on Ba-site reduces the rate of softening of this mode with compositional change, which could be attributed to the increased covalent nature of Ca–O bonds.

An ideal (primitive $Pm\bar{3}m$) cubic ABO_3 perovskite structure does not permit any Raman active mode in its first-order vibrational spectra; since each ion is at an inversion center and all long-wavelength vibrational modes are of odd parity. However many complex perovskites like PFN exhibit first-order Raman spectra over a wide temperature range.[20] Higher modes vary in complex perosvkite compounds as a function of the perovskite unit cell and the changes in the ionic radii. Thus, these high frequency modes have been found to be sensitive towards the change in the local crystal symmetry related to the presence of polar nano regions.[21] Although neither A, B′, nor B″ ions move in this A_{1g} vibration, the mode still reflects subtle changes in the perovskite structure. Only the oxygen ions move, but their spacing and bonding and, hence, frequencies change

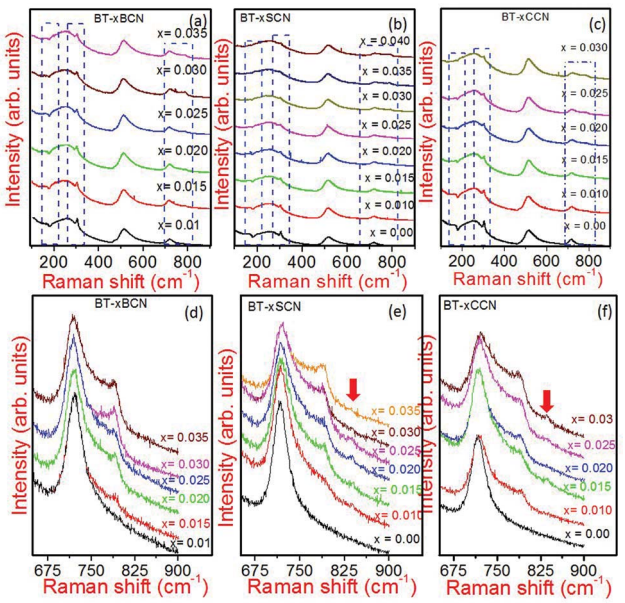

Fig. 7 Raman spectra recorded at RT for various compositions of (a) BT-*x*BCN, (b) BT-*x*SCN, (c) BT-*x*CCN. High frequency Raman modes at RT for (d) BT-*x*BCN, (e) BT-*x*SCN and (f) BT-*x*CCN.

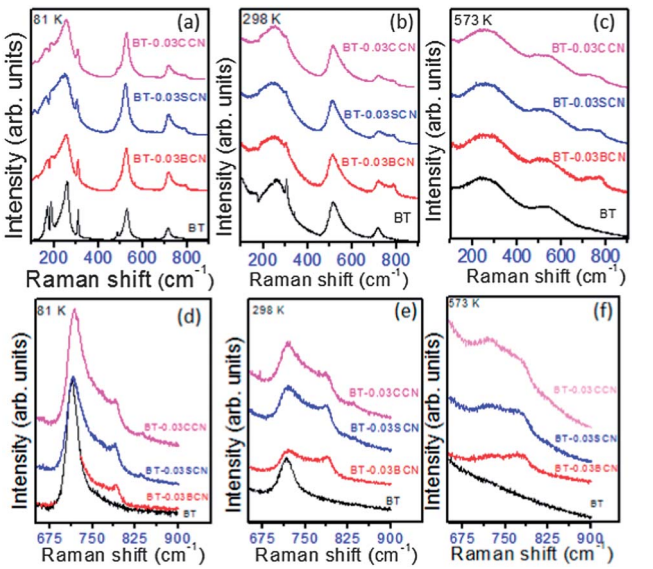

Fig. 8 Raman spectra of various compositions at (a) 81 K, (b) 298 K and (c) 573 K. Magnified high frequency regime for various compositions at (d) 81, (e) 298 and (f) 573 K.

with the size of the other ions involved. The lower Raman band 720 cm^{-1} corresponds to Ti–O stretching whereas the 792 cm^{-1} band represents Nb–O stretching.[22] In such system the vibration associated with two band modes do not couple due to their different chemical origin. The appearance of a mode at 792 cm^{-1} was considered as local counterpart of the $A_1(LO_3)$ mode appearing at 720 cm^{-1} in pure BT and is related to the internal deformation of the BO_6 octahedra due to the different cation substitutions on B site. The difference in the ionic radii of Cu^{2+} (0.73 A) and Nb^{5+} (0.64A) substituted on Ti^{4+} (0.605A) site would give rise to elastic dipole like distortion in the surrounding region. Moreover, a small mode observed at high frequency 840 cm^{-1} (marked with arrow) could be attributed to local modes of distorted octahedra due to substitution of Sr and Ca on the A-sites, because this mode was found to be absent in BT-*x*BCN. The appearance of new modes in the Raman spectra of modified BT has been interpreted as a presence of localized region with lower symmetry,[23] which sometimes is referred as polar nano regions giving rise to a diffuse nature of the phase transitions.

To further analyze the splitting of the high frequency modes in various compositions, their magnified view is shown in Fig. 7(d)–(f) for BT-*x*BCN, BT-*x*SCN and BT-*x*CCN, respectively. It can be seen that the mode due to TiO_6 octahedra is sharp in the case of BT-*x*BCN and is rather diffuse in the case of substitution of Sr^{2+} and Ca^{2+} on Ba^{2+}-site suggesting increased damping due to enhanced phonon anharmonicity. Moreover, the ratio of the intensities of modes corresponding to TiO_6 octahedra and NbO_6 octahedra decrease with the substitution of Sr^{2+} and Ca^{2+} on the Ba-site. Therefore, we observed that such a small substitution on A-sites perturbs the octahedral dynamics. These kinds of local distortions due to substitution on the Ba-sites make the atoms surrounding these sites to coherently shift away from the octahedra centers resulting in nucleation of small polar clusters or regions.[24] The ferroelectric active Nb^{5+} ions are more involved in this process leading to a significant distortion of the B-site cation shell of Ba^{2+}, Sr^{2+} and Ca^{2+} ions when surrounded predominantly by Nb^{5+} [ref. 24]. This is reflected in the appearance of new high frequency Raman modes.

The B-site substituted by Nb^{5+} ions are more covalently bound to oxygen than Ti^{4+} ions and Cu^{2+} ions resulting in a strong off-centered axially perturbed octahedral crystal field. This perturbation can also be seen in A_{1g} modes of Raman spectra of all the investigated systems. This can be rationalized by considering that atomic positional disorder in general; and of niobium and copper in particular at the lower concentration of Cu^{2+} and Nb^{5+}. The disorder increases as the population of polar to non-polar phase evolves. The perturbation of nano-polar regions is higher with increased concentration of B-site transition metal ions. Raman analysis also indicates an increase in the spatial range to which local tetragonal distortions can propagate coherently with increase in B-site substitutions which in turns increases the mean free path of the phonons associated with polar distortions. It is interesting to note that such a small compositional changes substantially modulates the local dynamics and distortions favoring a piezoelectric response. The PDF analysis also revealed enhanced polar distortions with the increase in the B-site substitution, which was further modulated by substitution of Ca and Sr.

To understand the nature of the phonon instabilities with the change in temperature, Raman spectra for pure $BaTiO_3$ (BT) and BT-0.03BCN, BT-0.03SCN and BT-0.03CCN were recorded in the temperature range of 81–573 K with 20 K interval. The low frequency mode observed at 305 cm^{-1} and high frequency mode at 720 cm^{-1} vanishes above the Curie temperature in pure $BaTiO_3$. Comparative plots of Raman spectra at various temperatures for pure $BaTiO_3$ and BT-0.03BCN, BT-0.03SCN and BT-0.03CCN are shown in Fig. 8(a)–(c). In order to investigate the effect of temperature on the local dynamics of TiO_6 and NbO_6 octahedra, a magnified view of the high frequency modes at 81, 298 and 573 K is shown in Fig. 8(d)–(f). From these spectra the following observations can be made: (i) The Raman modes get smeared with the substitution of Cu and Nb on Ti-site, with a further broadening when Sr^{2+} and Ca^{2+} are substituted on the Ba-sites, as observed in Fig. 8(a) and (b). Also, the monotonous suppression of the mode at 305 cm^{-1} at 81 and 298 K suggests a reduction of the long range ferroelectric ordering in the following sequence: BT > BT-*x*BCN > BT-*x*SCN > BT-*x*CCN. (ii) Though the Raman mode at 305 cm^{-1} vanishes, the high frequency modes at 720 and 792 cm^{-1} persist up to much higher than the Curie temperature indicating presence of polar nano regions. (iii) In the case of all three modified compositions, the intensity of both high frequency peaks decreases with the increase in *x*. However, in the case of BT-*x*BCN the rate of decrease in the intensity of the mode due to NbO_6 octahedra is lower than that of TiO_6 octahedra and, consequently, the corresponding Raman mode has a stronger intensity at 573 K. This phenomenon could be attributed to the NbO_6 moieties,[25] which play the role of stable pillar for the structure. (iv) The weak mode observed at 840 cm^{-1} at 298 K is more pronounced at low temperature of 81 K. Though this mode is absent in the high temperature spectra at 573 K for all compositions stressing its relation with the local octahedral distortions. (v) Appearance of a new mode at low frequency of 113 cm^{-1} in the case of all the modified compositions in the low and high temperature regime (up to 573 K). This mode is not very clear near room temperature probably due to the increase in intensity of the over-damped transverse mode. The observation of this mode in BT-*x*BCN (do not have A-site substitution), suggests that its origin is in the perturbation of phonon dynamics due to the B-site substitutions. The appearance of a similar lower frequency mode has been attributed to localized regions with rhombohedral local symmetry.[26] These localized polar regions or nano polar regions play an important role towards enhanced piezoelectric response of the specimen and result in diffuse nature of the phase transitions (DPT)[ref. 4]. Information about the local crystal field around Cu^{2+} is important for understanding the localized distortions and defect structure. Fortunately Cu^{2+} ions have unfilled d-orbitals, which make them EPR active.

Magnetically diluted Cu^{2+} centers ($3d^9$) with an electron spin $S = 1/2$ can be represented by a spin Hamiltonian:[27] $H = \mu_B B_o g S - \mu_n g_n B_o I + SAI$, where g_n is the corresponding nuclear

g factor and μ_B and μ_n are the Bohr and nuclear magnetons, respectively. The first term represents the electronic, while second term represents the Zeeman interactions and B_o denotes the external field. The third term corresponds to copper hyperfine interaction with $I^{Cu} = 3/2$ for both copper isotopes. X-band EPR spectra recorded at room temperature (RT) for samples having lower ($x = 0.01$) and higher ($x = 0.03$) concentration form BT-xBCN, BT-xSCN and BT-xCCN series are shown in Fig. 9(a) and (b), respectively. The shape of the EPR spectra is characteristic of axially distorted octahedral copper(II) ($3d^9$, S = 1/2, I = 3/2) complexes at RT. The EPR spectra contained two major peaks, corresponding to $g_{\|}$, which was split into four peaks due to hyperfine interactions with the copper(II) nucleus (I = 3/2), and $g_{\perp}$, which was the sharp central feature in the spectrum. This confirms the Cu^{2+} ($3d^9$) oxidation state of copper. Copper has two isotopes with natural abundances Cu^{63}: 69.09% and Cu^{65}: 30.91%, but both isotopes possess similar magnetic moment and a nuclear spin I = 3/2, giving rise to a nearly identical EPR signal.[27] From the EPR spectra, we noticed that the hyperfine lines ($g_{\|}$) are relatively sharp for the BT-xBCN specimens (BT-0.01BCN and BT-0.03BCN), and become rather smeared for the compounds having Sr^{2+} and Ca^{2+} on Ba^{2+}-site, which suggests local distortion created by this isovalent substitution coming from the different ionic radii and type of bonding. Likewise, the central peak corresponding to $g_{\perp}$ also appeared to contain hyperfine splitting (encircled region in the higher magnetic field regime of Fig 9(a) and (b)), which was more pronounced for the Ca^{2+} than for the Sr^{2+} or Ba^{2+}-sites suggesting enhanced distortion in crystal field, which is in line with the PDF results suggesting enhanced polar nature of this specimen at local length scales. According to first principal studies, having small ionic radii, Ca^{2+} has tendency to shift off-centering position in the AO_{12} dodecahedra due to its smaller ionic radius resulting in local polarization in the A-site of the perovskite structure.[28] Therefore, the effect of A-site substitution clearly supports formation of local regions with enhanced polar distortion as confirmed through EPR, Raman spectra and PDF analysis. Since in a powder sample, we observed only an averaged EPR spectrum due to the random orientation of the crystallites, the so called parallel and perpendicular orientations were only observed. By nature, the parallel part of the spectrum remains much weaker than the perpendicular part of the EPR spectrum and, hence, the observed EPR spectra conforms to the axial symmetry of the copper complex *i.e.* $g_x = g_y = g_{\perp}$ and $g_z = g_{\|}$. In the present case, $g_{\|} = 2.302$ and $g_{\perp} = 2.01$. The value of the hyperfine splitting constant $a_{\|} = 101$G. The values of the g factor were found to vary as $g_{\|} > g_{\perp} > 2$, which suggests that the ground state of the Cu^{2+} ion in the distorted octahedral (tetragonal) complex is $dx^2 - y^2$ [ref. 29]. Measured values of $g_{\|}$ and $g_{\perp}$ are characteristic of Cu^{2+} coordinated by six ligands that form an octahedron elongated by tetragonal distortion along its c-axis.[30] The observed distorted octahedral symmetry of the copper complexes suggests that copper occupies Ti^{4+} site with divalent oxidation state (Cu^{2+}), which results in a lowering of the local symmetry due to the Jahn–Teller effect,[27]

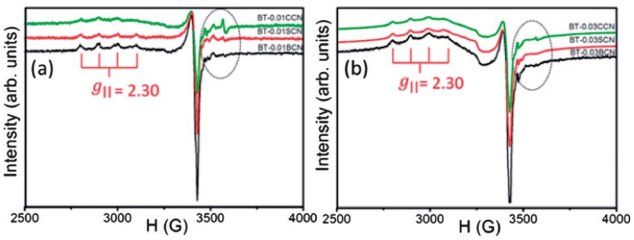

Fig. 9 EPR spectra recorded at RT for (a) $x = 0.01$ and (b) $x = 0.03$ compositions of different series.

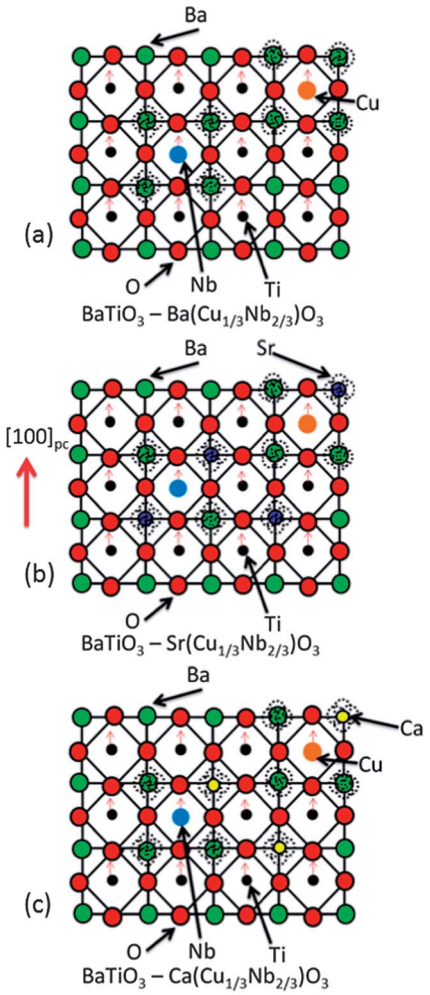

Fig. 10 Schematic showing (a) the Ba-site off-centering leading to local polar distortion due to increased repulsive interaction, (b) distortion due to substitution of Sr on Ba-site with B-site partially occupied with Nb and Cu, (c) distortion due to substitution of Ca on Ba-site with B-site partially occupied with Nb and Cu. The dotted circles are showing displacement of A-site cation due to A and B-site substitutions.

which supports formation of polar nano regions as discussed in Raman analysis. The random distribution of these structural distortions leads to averaging of anisotropy energy, and ease in the polarization rotation[31] giving rise to enhanced permittivity and piezoelectric response (Fig. 3 and 4).

Guidance for design of lead-free materials

In BT-xBCN, with the increase in the value of x, the piezoelectric response was found to increase up to $x = 0.025$ and then started to decrease. The trends of variations in piezoelectric response, with respect to change in the value of x, were similar to BT-xSCN and BT-xCCN series, however, the maximum occurred at different values of x (0.015 for BT-xSCN and 0.02 for BT-xCCN). The substitution of Nb and Cu on the Ti-site in $BaTiO_3$ increases the piezoelectric response initially due to the donor doping, however, on further increase in the Nb and Cu concentration the grain size decreases, which leads to the geometrical confinement of domains resulting in reduced piezoelectric response. The PDF, Raman and EPR results suggest that for lower concentration of doping, B-site substitutions enhance the polar nature considerably as illustrated through enhanced polar distortions, appearance of new Raman modes due to the perturbation of local dynamics and hyperfine splitting. With increasing concentration, Raman analysis indicated an increase in the spatial range to which local tetragonal distortions can propagate coherently with increase in B-site substitutions which in turns increases the mean free path of the phonons associated with polar distortions. The variation in properties is thus a balance of polar distortion, distribution of polar nano-regions, and domain confinement.

The substitution on A-site of $BaTiO_3$ by Sr and Ca was found to result in interesting variations in piezoelectric response. The substitution of small concentration of Sr on Ba-site (in BT-0.015SCN) was found to increase the long range order along with local polar distortions as observed in PDF results. However, increased concentration was found to reduce the local polar distortion. On the other hand, substitution of Ca on Ba-site (in BT-0.015CCN) was found to decrease the polar distortion first, though, for increased concentration of Ca (in BT-0.030CCN) polar distortion was found to remerge, which might be due to the partial substitution of Ca Ti-site since Ca has a smaller ionic radius in 6-fold coordination. However, the reduced grain size of the Ca-substituted specimen resulted in reduced piezoelectric response. The Raman and EPR results clearly indicate that not only aliovalent substitution on B-site, but also, A-site substitution results in local polar distortions with lower symmetry (polar nano regions). In all the three series of compositions the T_c and tetragonality (c/a) was found to decrease linearly with increase in the value of x. The slope of change in T_c with respect to x (dT_c/dx) was found to be -1210 (12.1 K/at%), -1424 (14.2 K/at%) and -1895 (18.9 K/at%) for BT-xBCN, BT-xSCN and BT-xCCN series of compositions. The magnitude of dT_c/dx was found to be highest for Ca modification (CCN) and lowest for Ba modification (BCN). The substitutions of Sr and Ca on A-site in pure $BaTiO_3$ have been found to decrease T_c [ref. 2], which was attributed to the reduced B-site off centering due to the smaller size of these atoms. Thus, the substitution of Ca on Ba-site not only reduces the piezoelectric response but also the rate of decrease in T_c was higher. The monotonous decrease in the T_c and tetragonality could be the result of reduced B-site off-centering due to the substitution of Ca and Sr on Ba-site.

The increased polar distortion due to Nb and Cu ion substitution can be attributed to the formation of local polar region with lower symmetry as discussed earlier. The substitution of larger ions Nb (ionic radii = 0.69 Å) and Cu (ionic radii = 0.73 Å) on Ti-site (ionic radii = 0.605 Å) will have higher repulsive interaction between Ba– Nb and Ba–Cu than Ba–Ti (the values of ionic radii are in six-fold coordination) (Fig. 10). These substitutions are expected to promote A-site off centering resulting in lower local symmetry (as discussed in PDF, Raman results and EPR results) and enhanced piezoelectric response. The situation becomes more complex in the case of substitution of Sr (ionic radii = 1.44 Å) and Ca (ionic radii = 1.34 Å) on Ba-site (ionic radii = 1.61 Å) [the ionic radii of A-site substituted elements are in 12-fold coordination] (Fig. 10). Smaller size of Sr and Ca will result in reduced repulsive interaction with B-site cation and could also result in increased polar distortion. However, the higher concentration of these ions might reduce the B-site off-centering resulting in a decrease in long range polar ordering. The increased concentration of aliovalent substitution on B-site is expected to result in the formation of point defects which consequently pin the grain boundary migration resulting in smaller grain size. Therefore, for increased value of x, if one can control the grain size and tailor the local structure to exhibit reduced symmetry then enhanced piezoelectric response with reduced rate of decrease in T_c might be expected. The strain effect in thin films has been found to increase the Curie temperature appreciably, unfortunately in the present case, the strain effect due to substitution of various elements was not sufficient to enhance the T_c. From the above discussion, it appears that the substitution of larger ion on Ba-site might lead to higher T_c due to strain effect. The results indicate that in order to realize high piezoelectric response through substitutional solid solution route, one needs to find appropriate A- and B-site ions such that the intrinsic lattice distortion is maximized, local scale structure exhibits reduced symmetry, and synthesis process results in the formation of microstructure that exhibits large grain size.

Conclusions

Series of new lead-free piezoelectric $(1-x)BaTiO_3$-$xA(Cu_{1/3}Nb_{2/3})O_3$ (A: Sr, Ba and Ca) ceramics were synthesized with high piezoelectric response. The substitutions of Nb and Cu on the B-site in $BaTiO_3$ increases the piezoelectric response in the initial stages, however, on further increase in the Nb and Cu the grain size decreases, which consequently leads to a geometrical confinement of domains resulting in reduced piezoelectric response. The substitution of small concentration of Sr on Ba-site (in BT-0.015SCN) was found to increase the piezoelectric response due to enhanced local polar distortions. The substitution of Ca on Ba-site (in BT-0.015CCN) was found to initially decrease the polar distortion, though, for increased concentration of Ca (in BT-0.030CCN) polar distortion was found to remerge. These substitutions promoted the A-site off-centering resulting in lower local symmetry due to the interplay between

the ionic radii and repulsive interactions. However, higher concentration of substituents was found to reduce the B-site off-centering resulting in a decrease in long range polar ordering (decrease in tetragonality) and reduction in the Curie temperature (T_c). Thus, by selecting proper ionic radii ratio and by controlling the grain size, one could achieve enhanced piezoelectric response with relatively higher Curie temperature.

Acknowledgements

The authors gratefully acknowledge the financial support from National Science Foundation (S.P.) and Office of Basic Energy Science, Department of Energy (D.M. (through #DE-FG02-07ER46480), Microscopy analysis and atomic PDFs analysis). The authors would also like to acknowledge the support from KIMS (design of new piezoelectric compositions).

References

1 K. Uchino, *Ferroelectric Devices*, 2009, CRC Press, 2009.
2 B. Jaffe, W. R. Cook and H. Jaffe, *Piezoelectric Ceramics*, Academic, New York, 1971.
3 L. E. Cross, Relaxor ferroelectrics, *Ferroelectrics*, 1987, **76**, 241.
4 G. A. Samara and E. L. Venturini, *Phase transitions*, 2006, **79**, 21.
5 T. Qi, I. Grinberg and A. M. Rappe, *Phys. Rev. B: Condens. Matter Mater. Phys.*, 2010, **82**, 134113.
6 I. Grinberg, V. R. Cooper and A. M. Rappe, *Nature*, 2002, **419**, 909.
7 S. Priya, A. Ando and Y. Sakabe, *J. Appl. Phys.*, 2003, **94**, 1171.
8 H. Taniguchi, H. Ping Soon, T. Shimizu, H. Moriwake, Y. Jin Shan and M. Itoh, *Phys. Rev. B: Condens. Matter Mater. Phys.*, 2011, **84**, 174106.
9 D. Maurya, N. Wongdamnern, R. Yimnirun and S. Priya, *J. Appl. Phys.*, 2010, **108**, 124111.
10 U. M. Pasha, H. Zheng, O. P. Thakur, A. Feteira, K. R. Whittle, D. C. Sinclair and I. M. Reaney, *Appl. Phys. Lett.*, 2007, **91**, 062908.
11 M. N. Rahaman and R. Manalert, *J. Eur. Ceram. Soc.*, 1998, **18**, 1063.
12 H. T. Langhammer, T. Müller, R. Böttcher and H.-P. Abicht, *Solid State Sci.*, 2003, **5**, 965–971.
13 S. H. Yoon and H. Kim, *J. Mater. Res.*, 2001, **16**, 1479.
14 V. Petkov, *Mater. Today*, 2008, **11**, 28.
15 V. Petkov, V. Buscaglia, M. T. Buscaglia, Z. Zhao and Y. Ren, *Phys. Rev. B: Condens. Matter Mater. Phys.*, 2008, **78**, 054107.
16 J. G. Bednorz and K. A. Müller, *Phy. Rev. Lett.*, 1984, **52**, 2289.
17 P. G. Clem, D. A. Payne and W. L. Warren, *J. Appl. Phys.*, 1995, **77**, 5865.
18 H. Richer, Z. P. Wang and L. Ley, *Solid State Commun.*, 1981, **39**, 625.
19 M. S. Chen, Z. X. Shen, S. H. Tang, W. S. Shi, D. F. Cui and Z. H. Chen, *J. Phys.: Condens. Matter*, 2000, **12**, 7013.
20 M. Correa, A. Kumar, S. Priya, R. S. Katiyar and J. F. Scott, *Phys. Rev. B: Condens. Matter Mater. Phys.*, 2011, **83**, 014302.
21 F. Jiang, S. Kojima, C. Zhao and C. Feng, *Appl. Phys. Lett.*, 2011, **79**, 3938.
22 A. Slodczyk and P. Colomban, *Materials*, 2010, **3**, 5007.
23 A. Slodczyk, P. Daniel and A. Kania, *Phys. Rev. B: Condens. Matter Mater. Phys.*, 2008, **77**, 184114.
24 N. Waeselmann, B. Mihailova, B. J. Maier, C. Paulmann, M. Gospodinov, V. Marinova and U. Bismayer, *Phys. Rev. B: Condens. Matter Mater. Phys.*, 2011, **83**, 214104.
25 A. Slodczyk and P. Colomban, *Materials*, 2010, **3**, 5007.
26 J. Kreisel, P. Bouvier, M. Maglione, B. Dkhil and A. Simon, *Phys. Rev. B: Condens. Matter Mater. Phys.*, 2004, **69**, 092104.
27 A. Abragam and B. Bleaney, *Electron Paramagnetic Resonance of Transition Ions*, Clarendon, Oxford, 1970.
28 T. Shimizu, D. Fu, H. Taniguchi, T. Taniyama and M. Itoh, *Appl. Phys. Lett.*, 2012, **100**, 102908.
29 J. W. Orton, *Electron Paramagnetic Resonance (An Introduction to Transition Group Ions in Crystal)*, London Iliffe Books, Ltd., London, 1968.
30 I. Yamada, M. Nishi and J. Akimitsu, *J. Phys.: Condens. Matter*, 1996, **8**, 2625.
31 T. Egami, Local atomic structure and large piezoelectric response, *Proceedings of the 2000 12th IEEE International Symposium on Applications of Ferroelectrics*, 21 Jul 2000–02 Aug 2000, vol. 1, pp. 273–278, DOI: 10.1109/ISAF.2000.941554.

